DOI 10.24425/aee.2025.153905

Implementation of a new active power filter control algorithm in time domain for selected current harmonics

DAWID BUŁA [1]✉, JAROSŁAW MICHALAK [1], TOMASZ KAMLER [2]

[1] *Faculty of Electrical Engineering, Silesian University of Technology, Poland*

[2] *Rabbit Sp. z o.o., Poland*

e-mail: ✉ *dawid.bula@polsl.pl*

(Received: 10.09.2024, revised: 17.04.2025)

Abstract: This paper presents a specific time domain algorithm for controlling an active power filter and its implementation. The proposed control algorithm is characterized by independent current control in each phase and the ability to select specific current harmonics generated by the active power filter. The chosen method of determining harmonics allows compensating for time delay in the control system. This ensures high harmonic reduction effectiveness and stable system operation in a wide frequency range, both in open and closed-loop control. The algorithm was implemented and tested in a real system with a digital controller based on a multi-core DSP microcontroller.

Key words: active power filter, harmonic detection, harmonic reduction, power quality, time delay compensation

1. Introduction

Higher harmonics in distribution networks can significantly affect the power quality [1–4]. The higher harmonics of current and voltage cause several adverse effects, such as power network overloads, generator and transformer overloads, insulations and capacitors ageing, production downtimes and failures [1–4]. As a result of the distorted currents, higher harmonics appear in voltage waveforms, affecting the operation of sensitive devices or protective devices used in electrical power systems. Using active power filters (APFs) [5–24] is one of the methods of reducing the higher harmonics in power networks. These solutions have been known for several decades [5, 6, 18], becoming increasingly popular with technological progress. In addition to

harmonics reduction, the APF can compensate for reactive power and reduce the load unbalance in three-phase systems. Regardless of the APF configuration, determining the reference current (for shunt systems) is one of the factors influencing its effectiveness. This is usually achieved by appropriately processing the measured grid or load currents. Many methods exist for determining the reference currents in both the frequency and the time domain [6]. Regardless of the method, it is necessary to process the measured signals using mathematical operations appropriate for the chosen technique. Even in the fastest real-time systems, this processing takes time, which leads to delays.

In most cases, the delay effect in the reference determination process is acceptable but leads to harmonic damping effectiveness lower than the theoretical one. However, there are cases where this delay can affect the system's stability or significantly reduce the APF damping effectiveness. This happens, for example, in the case of closed-loop systems (based on the grid current measurement) and in the case of using the APF for higher-order harmonics reduction.

The paper proposes a control algorithm that allows the reduction of selected current harmonics and presents its implementation for a shunt active power filter. The algorithm is based on the time domain, ensures the APF operation in a closed-loop system and ensures independent operation of the APF for each phase. Independent control of phase current is crucial for three-phase, four-wire systems. It allows the reduction of selected harmonics with time delay compensation and the reduction of the fundamental harmonic reactive power. The control of the system was implemented based on the TMS320F28379D microcontroller.

Among the publications, one can find solutions that allow determining specific harmonics [7, 9–11, 13, 15, 20] and methods for compensating/reducing delays that occur in the processing chain [10, 11, 14, 17, 19, 24]. For example, work [20] presents a method of determining harmonics similar to the proposed one, i.e. based on the frequency response shift by Park transform. Importantly, in [20], it was shown that the method based on the Park transform can be equivalent to the recursive discrete Fourier transform and cascade delayed signal cancellation harmonic extraction can be equivalently realized by using the synchronous rotating frame-based structure. In [13], filter banks based on the Fourier series, called moving discrete Fourier transform, were proposed for determining selective harmonics. It is also worth mentioning article [11], in which the authors present an open-loop architecture for three-phase grid synchronization based on moving averages and predictive filters. In this solution, predictive filters are proposed to compensate for delays occurring in processing. Delay compensation was also shown in [14] when the authors used a solution called the multiple delayed signal cancellation (MDSC) for improving the dynamic performance of the conventional synchronous reference frame under adverse three-phase grid conditions.

Unlike the methods described in other papers, the presented method is characterized primarily by a low number of mathematical operations, which allows for its trouble-free implementation in real systems, as shown in this work. The presented control algorithm is a new solution that will be used in active power filters planned for commercial production.

2. Proposed algorithm for determining reference currents

The methods of determining harmonics in the time domain are characterised by mathematical operations, significantly affecting the required calculation time. The proposed method is based on the *dq* method modified to a single phase [15, 16, 23]. The method for single phases is necessary

to determine reactive power independently for each phase, as described in [15]. The standard approach in this case is to determine all higher current harmonics and the current associated with reactive power as shown in Fig. 1.

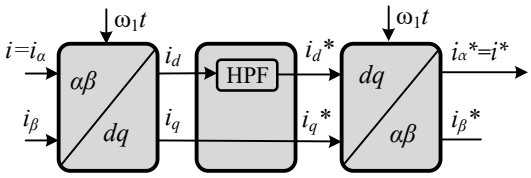

Fig. 1. Method of determining the reference current for higher harmonics and reactive power [15]

The input currents in this case are:

$$\begin{bmatrix} i_\alpha \\ i_\beta \end{bmatrix} = \begin{bmatrix} i(t) \\ i\left(t - \dfrac{T}{4}\right) \end{bmatrix}, \tag{1}$$

where $i(t)$ is the current of a given phase.

However, the dq transformation and the inverse transformation can be written in the form:

$$\begin{bmatrix} i_d \\ i_q \end{bmatrix} = \begin{bmatrix} \cos(\omega_1 t) & \sin(\omega_1 t) \\ -\sin(\omega_1 t) & \cos(\omega_1 t) \end{bmatrix} \begin{bmatrix} i_\alpha \\ i_\beta \end{bmatrix}, \tag{2}$$

$$\begin{bmatrix} i_\alpha^* \\ i_\beta^* \end{bmatrix} = \begin{bmatrix} \cos(\omega_1 t) & -\sin(\omega_1 t) \\ \sin(\omega_1 t) & \cos(\omega_1 t) \end{bmatrix} \begin{bmatrix} i_d^* \\ i_q^* \end{bmatrix}. \tag{3}$$

where ω_1 is the fundamental harmonic angular frequency.

The output current i_α^* is a reference current, and the HPF is a high-pass filter. In this method, there is no direct way of selecting current harmonics for reduction and no possibility of compensating for the resulting processing delays. That is why its modification was proposed, dividing the current reference into higher harmonic components and a reactive power component. Figure 2 shows a part of the algorithm responsible for determining the component related to reactive power. Figure 3 shows a part of the algorithm relevant to determining a reference for a specific current harmonic order (h).

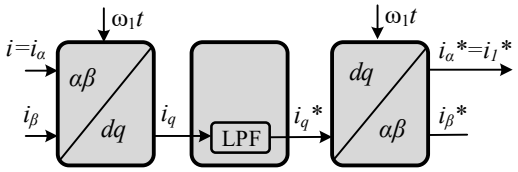

Fig. 2. Proposed method for determining the reference current for reactive power

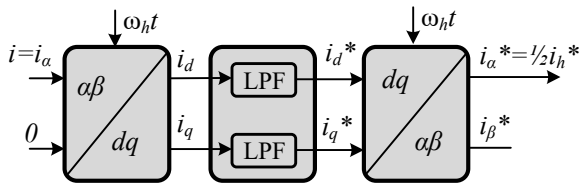

Fig. 3. Proposed method for determining the reference current for the selected harmonic

It should be noted that there is no need to transform the current i_β because there is no need of determining the specific harmonic component related to reactive power, therefore:

$$\begin{bmatrix} i_\alpha \\ i_\beta \end{bmatrix} = \begin{bmatrix} i\,(t) \\ 0 \end{bmatrix}, \tag{4}$$

$$\begin{bmatrix} i_d \\ i_q \end{bmatrix} = \begin{bmatrix} \cos(\omega_h t) \\ -\sin(\omega_h t) \end{bmatrix} [i_\alpha] \tag{5}$$

As a final result, i_α^* equals half of the reference current of a given harmonic i_h^* (Appendix A.1).

A single-phase simplified equivalent model shown in Fig. 4(a) was used to analyse the proposed algorithm in the frequency domain (for higher harmonics), i.e., to determine the frequency characteristics. The active power filter is represented here as a current source controlled by measured line current I_S. In Fig. 4(b) the model appropriate for the transfer function of the APF control system has been shown. It is assumed that voltage drop across the source impedance does not affect the load current, so the load is modelled as a current source.

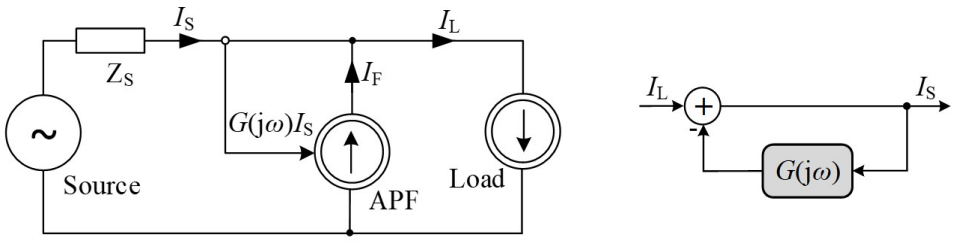

(a) (b)

Fig. 4. Mode used for frequency domain analyse: (a) single-phase simplified equivalent model; (b) control diagram

The transfer function $G(\mathrm{j}\omega)$ results from the following relationships:

$$I_F = K\,(\mathrm{j}\omega)\,I_L, \tag{6}$$

$$I_L = I_S + I_F, \tag{7}$$

so:

$$I_F = \frac{K\,(\mathrm{j}\omega)}{1 - K\,(\mathrm{j}\omega)} I_S = G\,(\mathrm{j}\omega)\,I_S. \tag{8}$$

The relationship between the grid current I_S and the load current I_L for higher harmonics (Fig. 4(b)) is:

$$\frac{I_S}{I_L} = \frac{1}{1 + G(j\omega)}. \tag{9}$$

The transfer function $K(j\omega)$ is the sum of the transfer functions for individual harmonics resulting from the control algorithm (Appendix A) and can be written in the form:

$$K(j\omega) = \sum_h \left[X(j\omega - j\omega_h) + X(j\omega + j\omega_h) \right], \tag{10}$$

where $X(j\omega)$ is the transfer function of the LPF filter, assuming the same filters for each harmonic.

An example of a frequency characteristic of this transfer function that allows extracting odd harmonics is shown in Fig. 5. It can be seen that the algorithm extracts the harmonics and the phase shift for a specific harmonic in the ideal case is zero. The characteristic shown in Fig. 5 depends on the low-pass filters used. It should be taken into account that the filter has sufficiently high attenuation for 100 Hz (range between successive harmonics), otherwise the magnitude value for the individual harmonics will be less than one. For the presented results, the second-order Butterworth filters with a cut-off frequency of 7 Hz have been used.

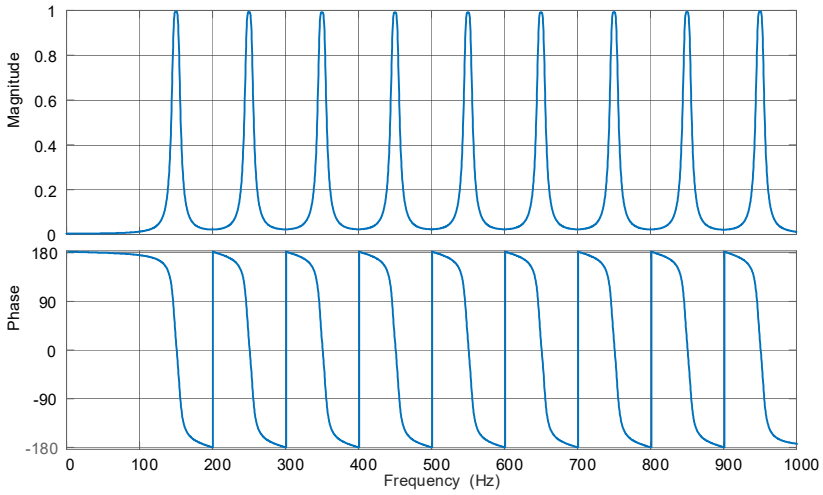

Fig. 5. Bode diagram for $K(j\omega)$ transfer function

The damping effect of higher harmonics, as a result of Eq. (9), is presented in Fig. 6. The damping for selected harmonics is clearly visible here.

It should be noted that in a real time system there are delays resulting from the delay in the measurement system and the finite processing time, as well as delays in the reference realization. These delays can be replaced by one common delay included in the transfer function $K(j\omega)$:

$$K(j\omega) = \left(\sum_h \left[X(j\omega - \omega_h) + X(j\omega + \omega_h) \right] \right) e^{-j\omega\tau}. \tag{11}$$

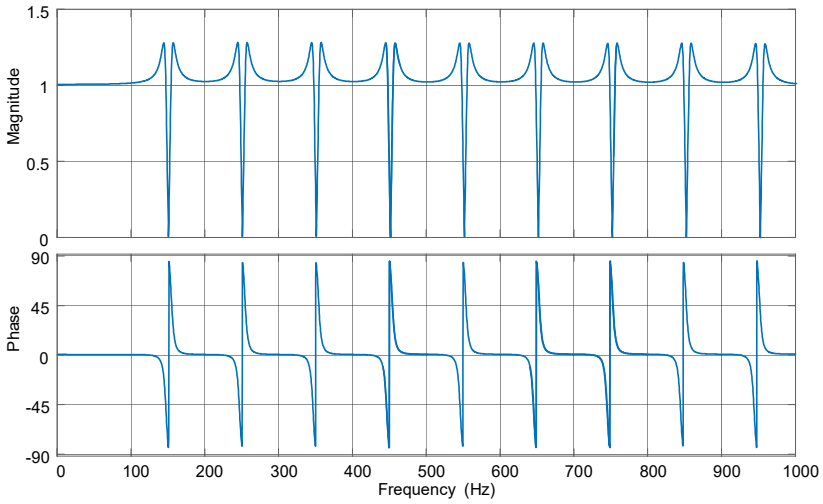

Fig. 6. Bode diagram for damping characteristic of the proposed method

Due to the time delay τ (a constant value of time delay is assumed here for each harmonic), the phase shift of the transfer function occurs. The order of the harmonic increases the phase shift, which is shown in Fig. 7.

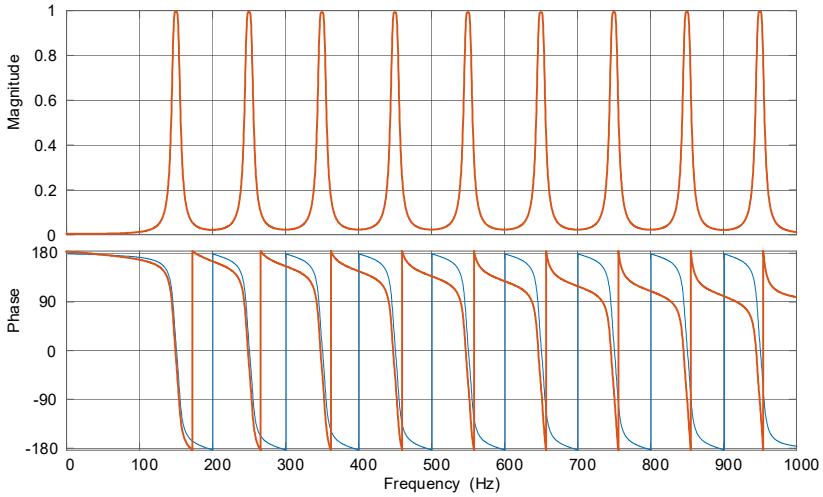

Fig. 7. Bode diagram for $K(\mathrm{j}\omega)$ transfer function in the case of taking into account the time delay (red) against the background of the Bode diagram without delays (blue–Fig. 5)

The phase shift primarily affects the accuracy of harmonic reduction but can also affect the system's stability. Due to the first or second-order low-pass filter used, the system shown in Fig. 4(a) is always stable. Figure 8(a) presents the Nyquist diagrams for the transfer function $G(\mathrm{j}\omega)$

(open-loop transfer function from Fig. 4(a)) for a system with no delay and an ideal case with a delay of 250 μs. However, in the case of the real system, e.g. with an additional capacitive load, the system loses stability even with a slight delay (8(b)). In this case, the higher harmonics of the load current strongly depend on the voltage drop across the source impedance.

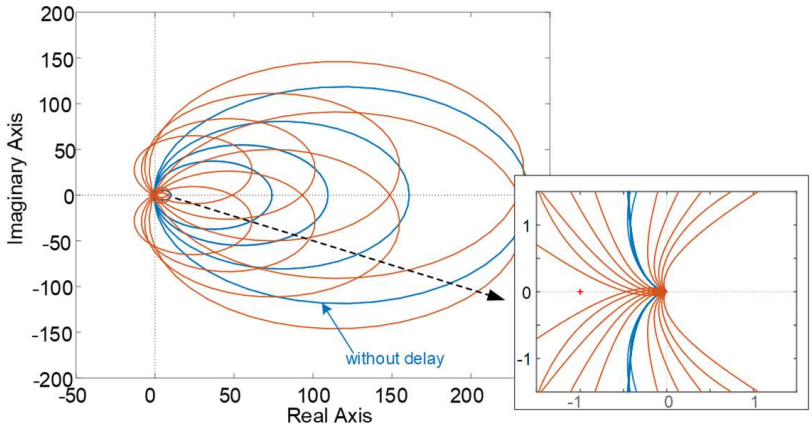

(a)

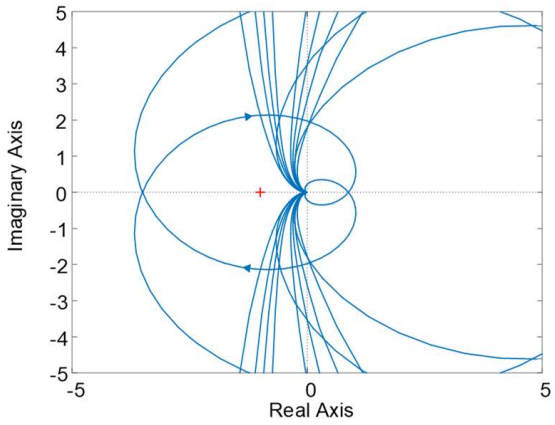

(b)

Fig. 8. Nyquist diagram for $G(j\omega)$ transfer function: (a) ideal case with delay $\tau = 250$ μs; (b) real case with capacitive load and delay $\tau = 75$ μs

Since in the proposed method, each harmonic is determined independently, it is possible to add a delay compensator (DC), shown in Fig. 9, which causes a phase shift for each harmonic. The equation for the compensator can be written in the form:

$$\begin{bmatrix} i_d^* \\ i_q^* \end{bmatrix} = \mathrm{DC} \begin{bmatrix} i_d' \\ i_q \end{bmatrix}, \tag{12}$$

$$\mathrm{DC} = \begin{bmatrix} \cos(\omega_h \tau) & -\sin(\omega_h \tau) \\ \sin(\omega_h \tau) & \cos(\omega_h \tau) \end{bmatrix}. \tag{13}$$

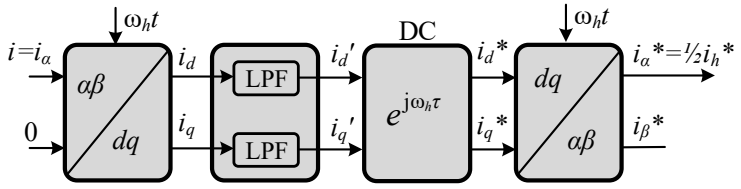

Fig. 9. Proposed method for determining the reference current for the selected harmonic with time delay compensation

The delay τ is constant in this case, but it can be dependent on the harmonic order, which is helpful in the case of compensation for a nonlinear phase shift in the measurement path.

Figure 10 shows the final, complete algorithm for determining the reference current of a single phase. The time delay compensation for the reactive power component is omitted here.

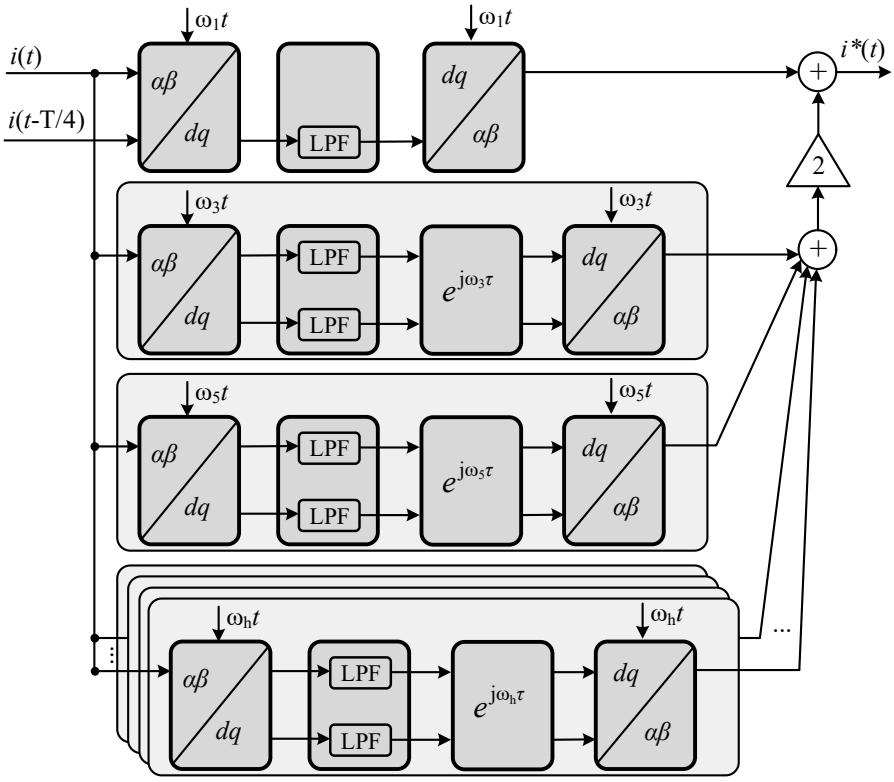

Fig. 10. Proposed method for determining the reference current for reduction of all selected harmonics and reactive power compensation

3. Implementation of an algorithm and laboratory results

The proposed algorithm has been implemented and tested in the prototype of a three-phase, four-wire active power filter presented in Fig. 11. The prototype of the APF is based on an ANPC (active neutral point clamped converter) [25] with a nominal current of 50 A (RMS). The ANPC topology uses both IGBT transistors and MOSFET transistors. The IGBT transistors are switched with fundamental frequency (50 Hz) and MOSFET with 50 kHz, and in this way it is possible to reduce power losses (Table 1). The APF ensures the reduction of reactive power and higher harmonics in each phase independently. The converter uses an LCL passive filter for damping current ripples caused by the switching of power modules. To ensure the high dynamics of the converter, an operation with a switching frequency of 50 kHz has been chosen. Such switching frequency and a 3-level converter reduce the value of passive elements in the LCL filter. The APF inner control loop uses grid voltages v_{Gabc} to control converter current i_{Cabc} and stabilizes the DC link voltages v_{DC}. The APF prototype is shown in Fig. 12 and its parameters are presented in Table 1.

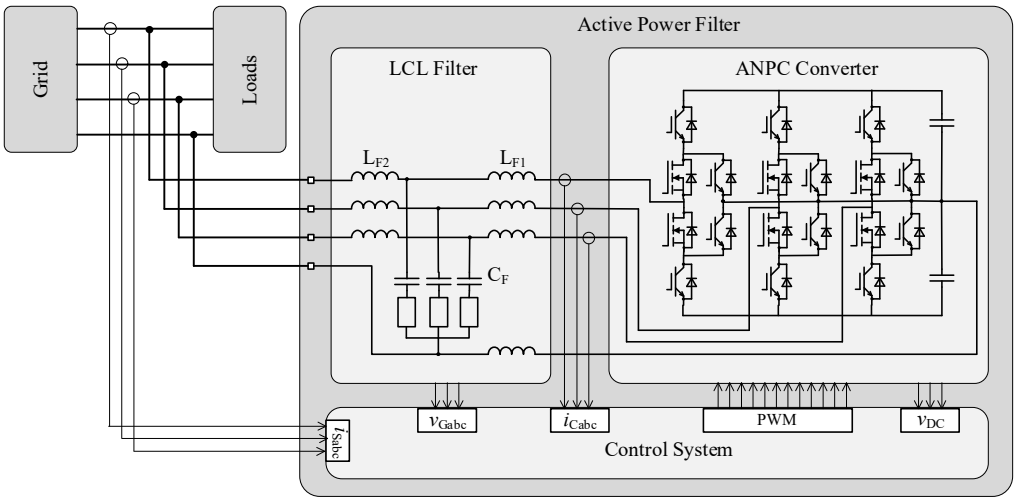

Fig. 11. Block diagram of the APF prototype

The control system of the APF is based on the TMS320F28376D DSP microcontroller, operating with 200 MHz clocking. The microcontroller has two independent CPUs (central processing unit) and two additional CLA (control law accelerator) coprocessors. Each of the cores uses a single precision floating point computation. The CLA coprocessors are useful for parallel computations, while the main CPU can perform other tasks. The main functions and task division are presented in Fig. 13. The CPU1 is responsible for communication (Modus RTU protocol), data exchange with an external database and power quality analysis (THD coefficients, RMS values, harmonics, etc.). These tasks are independent of the control system. The control algorithm and protections of the APF are implemented in the CPU2 processor. The control algorithm is responsible for synchronization to grid voltage, reference currents calculation (for harmonics and reactive power reduction), control of converter current, DC link voltage control, protections and

Table 1. The APF parameters

APF parameters	Value	Passive elements	Value
S_N nominal power	34.6 kVA	L_{F1} inverter side choke	150 mH
V_N nominal voltage	400 V	L_{F2} grid side choke	50 mH
I_N nominal current	50 A	C_F filter capacitor	2.2 mH
f_{sw} switching freq.	50 kHz	R_F damping resistor	1 Ω
P_{loss} total power losses	< 700 W	C_{DC} DC lick capacitor	6.6 mF
P_{closs} conv. power losses	< 550 W		

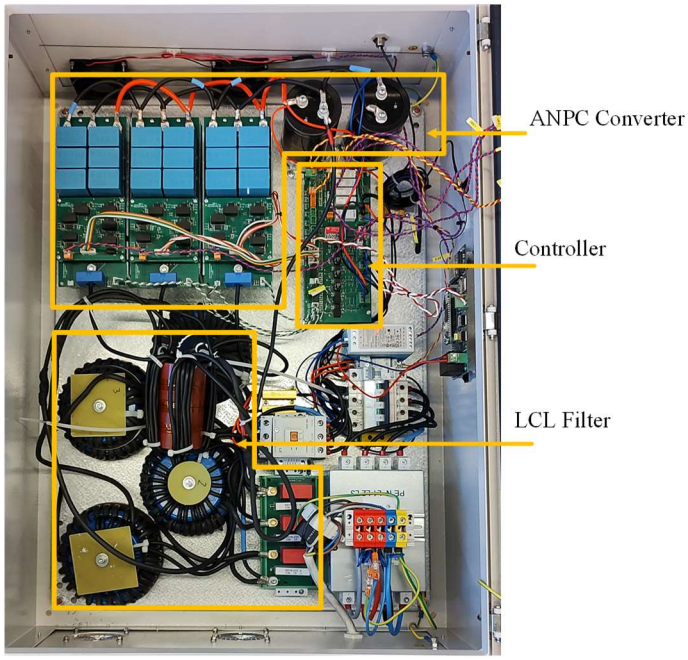

Fig. 12. Prototype of the active power filter

PWM control. Because the switching frequency f_{sw} = 50 kHz, all computations need to be done during a period of time lower than 20 μs, to determine the harmonics the CLA2 coprocessor has been used. To ensure proper operation of the APF and the longest time for the CLA2 computation in each iteration, the CPU2 reads the results of the previous computation. Then, it sends the new values for computation to the CLA2 coprocessor and starts a task in it. After that, the CPU2 finishes its control tasks. The delay time compensation is taken into account during determining the reference current (Fig. 9) for each phase and each harmonic independently. It must be mentioned that the proposed control algorithm with a determination of single current harmonics does not take a long time. However, if we consider that it is necessary to determine several harmonics for

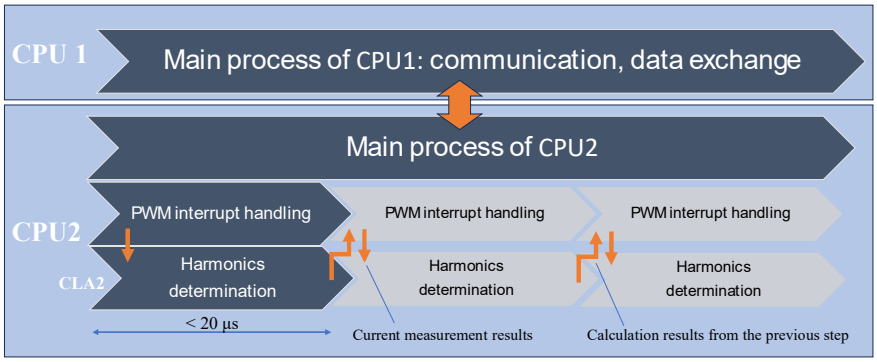

Fig. 13. Diagram of main functions and task division in DSP microcontroller

each phase independently, the computations must be repeated several dozen times. By proper optimization, the proposed method allows performing all required calculations for harmonics up to the 39th order in a period lower than 20 µs. The results of implementing the proposed control algorithm are presented in Figs. 14, 15, 16. They were collected for closed-loop control when the grid currents have been used as feedback signals.

Figures 14 and 15 present selected experimental results for typical single-phase and three-phase loads. Cases where currents with high harmonic content occur, were deliberately selected to show the performance and advantages of using the proposed algorithm. For both figures the results without and with delay compensation are shown. It can be seen that the effectiveness of damping of harmonics strongly depends on delay compensation. Table 2 presents harmonic content for both situations

Table 2. Harmonic content (in %, 1 – case without delay compensator, 2 – case with delay compensator)

Harmonic no.	**Single-phase load**			**Three-phase load**		
	i_{L}	$i_{\mathrm{S(1)}}$	$i_{\mathrm{S(2)}}$	i_{L}	$i_{\mathrm{S(1)}}$	$i_{\mathrm{S(2)}}$
3	81.6	4.4	0.6	1.0	1.1	1.2
5	66.5	6.9	2.6	69.7	6.5	0.5
7	44.5	6.7	1.7	46.0	5.0	0.6
9	18.0	3.3	0.9	1.0	0.3	0.2
11	6.1	1.6	0.9	9.5	1.3	0.4
13	2.9	0.2	0.4	2.1	0.1	0.6
15	5.4	2.0	0.9	0.1	0.4	0.4
17	2.6	1.5	0.6	2.9	1.2	0.9
19	0.5	0.4	0.1	1.0	1.0	0.8
THD	116.3	11.8	3.9	84.2	9.1	2.6

pictured in Figs. 14 and 15. One can see that for a single-phase load the THD current reduction was from 116.3% to 11.8% without delay compensation and to 3.9% with time delay compensation. For a three-phase load this reduction was from 84.2% to 2.6% with time delay compensation.

As it was mentioned previously, the independent reduction of current harmonics gives the possibility to reduce only selected harmonics. It can be helpful in the situation when a user would like to reduce the power of the APF or when it is possible to cause any operation instability in the case of resonances in the power system. An example of operation with a three-phase load when only 5th and 7th current harmonics have been selected in control system is presented in Fig. 16. For such a situation the RMS of current generated by the APF is lower and THD reduction was from 84,3% to 11.4%. It can be seen that only the selected harmonics have been reduced, and other harmonics can still be seen in the grid current. The presented results prove the proper operation of the APF with the proposed control algorithm.

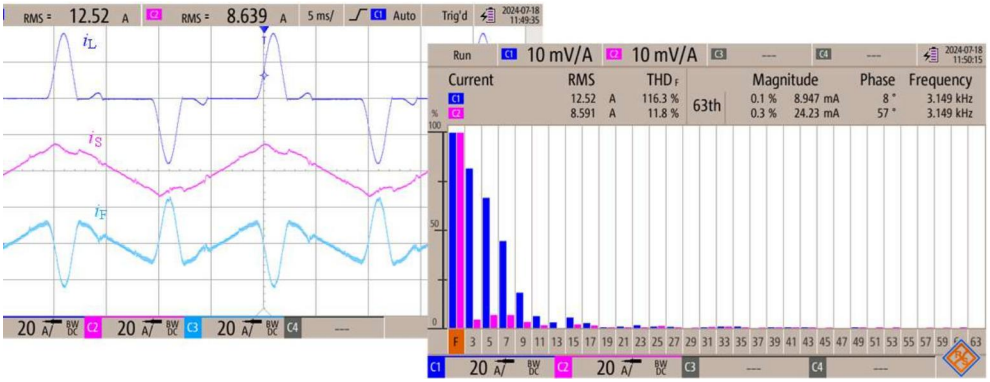

(a)

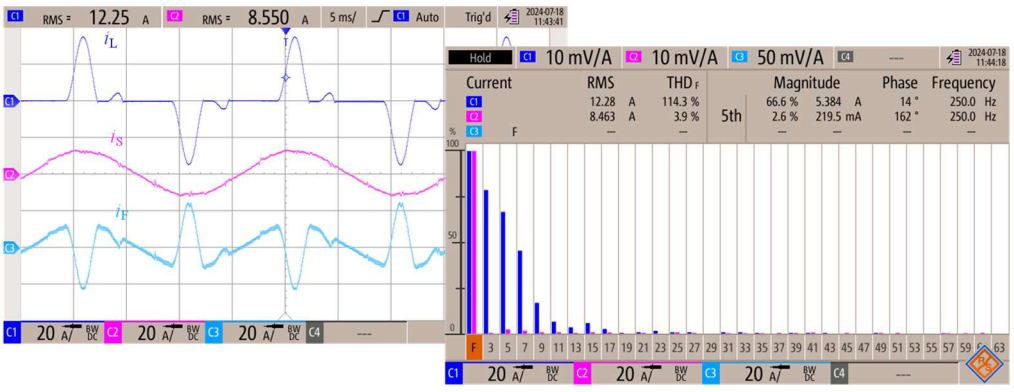

(b)

Fig. 14. Example experimental results for a single-phase load: a) case without the use of a delay compensator, b) case with the use of a delay compensator

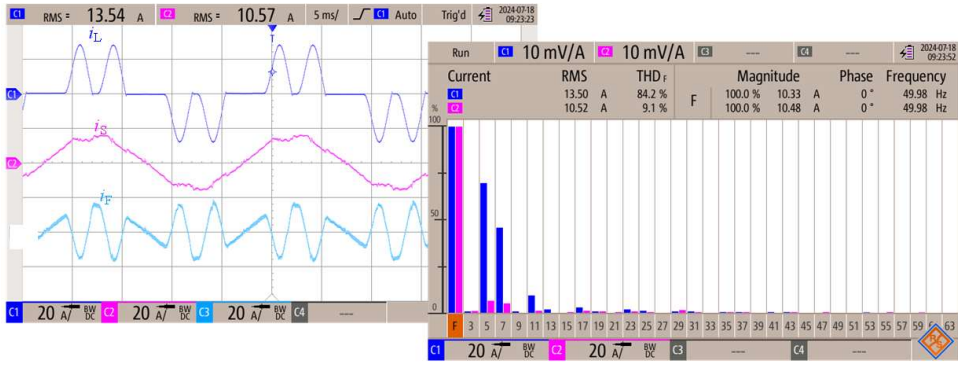

(a)

(b)

Fig. 15. Example experimental results for a three-phase load: (a) case without the use of a delay compensator; (b) case with the use of a delay compensator

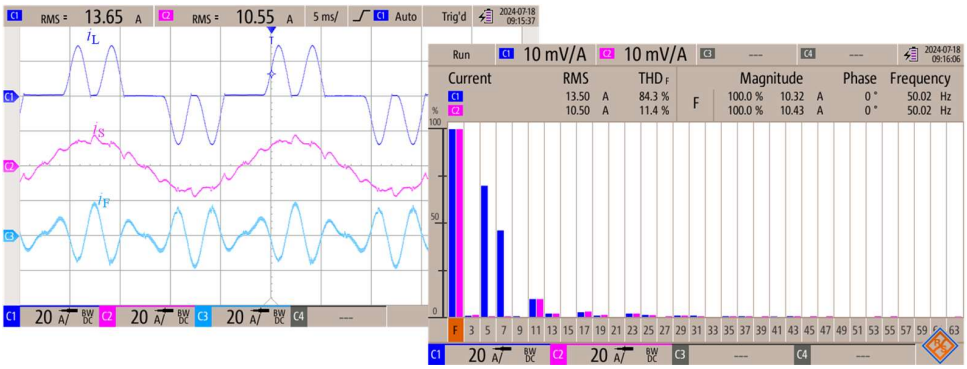

Fig. 16. Example experimental results for a three-phase load assuming 5th and 7th harmonic reduction (case with a delay compensator)

4. Conclusions

The proposed algorithm for determining the reference currents of the active power filter, presented in the paper, allows for the effective reduction of harmonics. This is confirmed by the experimental results obtained using the prototype of the APF with the ANPC converter presented in the paper. The determination of specific harmonics allowed the introduction of a delay compensator, which significantly impacts the harmonic-damping effectiveness of the active power filter. A simplified stability analysis showed that using a compensator also improves the system's stability. This method can be applied to various APF topologies, single- and three-phase (four-wire), with load and grid current measurements. The presented algorithm is being implemented in new active power filters introduced into commercial production. The theoretical derivations shown in the paper can be helpful in the analysis of other methods and algorithms using *dq* transformation.

Appendix

Proof of dependency (10) for the proposed method of determining the reference current for the selected harmonic (Fig. 3).

$$i_d(t) = \cos(\omega_h t)\, i(t), \tag{A.1}$$

$$i_q(t) = -\sin(\omega_h t)\, i(t). \tag{A.2}$$

Using the modulation property of Fourier transform we can write:

$$I_d(\mathrm{j}\omega) = \frac{1}{2}\left[I(\mathrm{j}\omega - \mathrm{j}\omega_h) + I\left(\mathrm{j}\omega + \mathrm{j}\omega_h\right)\right], \tag{A.3}$$

$$I_q(\mathrm{j}\omega) = -\frac{1}{2\mathrm{j}}\left[I(\mathrm{j}\omega - \mathrm{j}\omega_h) - I\left(\mathrm{j}\omega + \mathrm{j}\omega_h\right)\right], \tag{A.4}$$

and then:

$$I_d^*(\mathrm{j}\omega) = X(\mathrm{j}\omega)\frac{1}{2}\left[I\left(\mathrm{j}\omega - \mathrm{j}\omega_h\right) + I\left(\mathrm{j}\omega + \mathrm{j}\omega_h\right)\right], \tag{A.5}$$

$$I_q^*(\mathrm{j}\omega) = -X(\mathrm{j}\omega)\frac{1}{2\mathrm{j}}\left[I(\mathrm{j}\omega - \mathrm{j}\omega_h) - I\left(\mathrm{j}\omega + \mathrm{j}\omega_h\right)\right], \tag{A.6}$$

where $X(\mathrm{j}\omega)$ is the transfer function of the low pass filter.

The reference output current is:

$$i_\alpha^*(t) = \cos(\omega_h t)\, i_d^*(t) - \sin(\omega_h t)\, i_q^*(t). \tag{A.7}$$

which, after applying the modulation property, gives

$$I(\mathrm{j}\omega) = \frac{1}{2}\left[I_d^*(\mathrm{j}\omega - \mathrm{j}\omega_h) + I_d^*(\mathrm{j}\omega + \mathrm{j}\omega_h)\right] - \frac{1}{2\mathrm{j}}\left[I_q^*(\mathrm{j}\omega - \mathrm{j}\omega_h) - I_q^*\left(\mathrm{j}\omega + \mathrm{j}\omega_h\right)\right]. \tag{A.8}$$

By inserting Eqs. (A.5) and (A.6) into the above and rearranging, we finally get:

$$I_\alpha^*(\mathrm{j}\omega) = \frac{1}{2}I(\mathrm{j}\omega)\left[X\left(\mathrm{j}\omega - \mathrm{j}\omega_h\right) + X\left(\mathrm{j}\omega + \mathrm{j}\omega_h\right)\right], \tag{A.9}$$

which can be saved as:

$$I_{\alpha}^{*}(\mathrm{j}\omega) = \frac{1}{2} I(\mathrm{j}\omega) X'(\mathrm{j}\omega). \tag{A.10}$$

Examples of Bode diagrams of a low-pass filter $X(\mathrm{j}\omega)$ (2nd order Butterworth, $fc = 7$ Hz) and transfer function $X'(\mathrm{j}\omega)$ for $h = 7$ are shown in Fig. A.1.

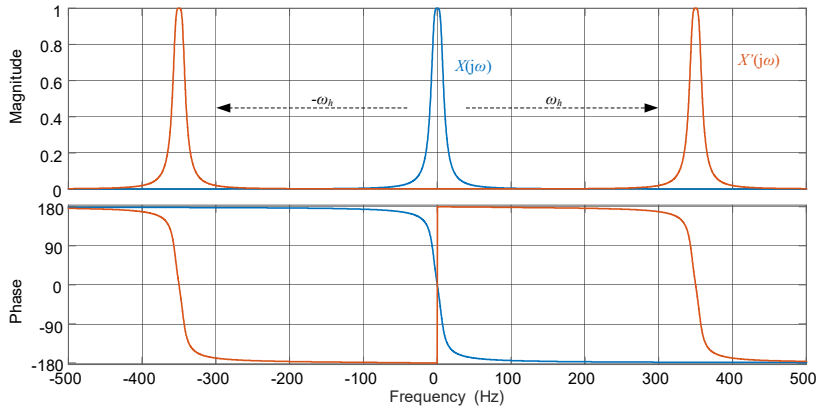

Fig. A.1. Bode diagram for transfer functions $X(\mathrm{j}\omega)$ and $X'(\mathrm{j}\omega)$

Acknowledgements

This research was partly financed by the EU funding for 2014–2020 within Smart Growth Operational Programme.

References

[1] Dugan R.C., Santoso S., McGranaghan M.F., Beaty H.W., *Electrical Power Systems Quality*, McGraw Hill Professional (2002).

[2] Kusko A., *Power Quality in Electrical Systems*, 1st Edition, McGraw-Hill Education (2007).

[3] Das JC., *Power System Harmonics and Passive Filter Designs*, John Wiley & Sons (2015).

[4] Beleiu H.G., Beleiu I.N., Pavel S.G., Darab C.P., *Management of Power Quality Issues from an Economic Point of View*, Sustainability, vol. 10, no. 7, (2018), DOI: 10.3390/su10072326.

[5] Singh B., Al-Haddad K., Chandra A., *A review of active filters for power quality improvement*, IEEE Transactions on Industrial Electronics, vol. 46, no. 5, pp. 960–971 (1999), DOI: 10.1109/41.793345.

[6] Asiminoael L., Blaabjerg F., Hansen S., *Detection is key - Harmonic detection methods for active power filter applications*, IEEE Industry Applications Magazine, vol. 13, no. 4, pp. 22–33 (2007), DOI: 10.1109/MIA.2007.4283506.

[7] Freijedo F.D., Doval-Gandoy J., Lopez Ó., Fernandez-Comesana P., Martinez-Penalver C., *A Signal-Processing Adaptive Algorithm for Selective Current Harmonic Cancellation in Active Power Filters*, IEEE Transactions on Industrial Electronics, vol. 56, no. 8, pp. 2829–2840 (2009), DOI: 10.1109/TIE.2009.2013844.

[8] Buła D., Pasko M., *Hybrid power filter with single tuned passive filter - dynamical properties*, 2010 International School on Nonsinusoidal Currents and Compensation, Lagow, Poland, pp. 80–83 (2010), DOI: 10.1109/ISNCC.2010.5524521.

[9] Neves F.A.S., de Souza H.E.P., Cavalcanti M.C., Bradaschia F., Bueno E.J., *Digital Filters for Fast Harmonic Sequence Component Separation of Unbalanced and Distorted Three-Phase Signals*, IEEE Transactions on Industrial Electronics, vol. 59, no. 10, pp. 3847–3859 (2012), DOI: 10.1109/TIE.2011.2163284.

[10] Wang Y.F., Li Y.W., *Three-Phase Cascaded Delayed Signal Cancellation PLL for Fast Selective Harmonic Detection*, IEEE Transactions on Industrial Electronics, vol. 60, no. 4, pp. 1452–1463 (2013), DOI: 10.1109/TIE.2011.2162715.

[11] Freijedo F.D., Doval-Gandoy J., López Ó., Acha E., *A Generic Open-Loop Algorithm for Three-Phase Grid Voltage/Current Synchronization with Particular Reference to Phase, Frequency, and Amplitude Estimation*, IEEE Transactions on Power Electronics, vol. 24, no. 1, pp. 94–107 (2009), DOI: 10.1109/TPEL.2008.2005580.

[12] Szromba A., *Conductance-controlled global-compensation-type shunt active power filter*, Archives of Electrical Engineering, vol. 64, no. 2, pp. 259–275 (2015), DOI: 10.1515/aee-2015-0022.

[13] Sozański K., *Three phase active power filter with selective harmonics elimination*, Archives of Electrical Engineering, vol. 65, no. 1, pp. 33–44 (2016), DOI: 10.1515/aee-2016-0003.

[14] Gude S., Chu C.-C., *Three-Phase PLLs by Using Frequency Adaptive Multiple Delayed Signal Cancellation Prefilters Under Adverse Grid Conditions*, IEEE Transactions on Industry Applications, vol. 54, no. 4, pp. 3832–3844 (2018), DOI: 10.1109/TIA.2018.2823263.

[15] Buła D., Jarek G., Michalak J., Zygmanowski M., *Control Method of Four Wire Active Power Filter Based on Three-Phase Neutral Point Clamped T-Type Converter*, Energies, vol. 14, no. 24 (2021), DOI: 10.3390/en14248427.

[16] Waqas M., Ahmed T., Elavarasan R.M., Waqar A., Leong K., Pugazhendhi R., Das N., Jeelani M.W., *DQ Transformation Based Control of Single-Phase Grid-Tied Inverter*, in 2021 31st Australasian Universities Power Engineering Conference (AUPEC) (2021), DOI: 10.1109/AUPEC52110.2021.9597712.

[17] Buła D., Michalak J., Zygmanowski M., Adrikowski T., Jarek G., Jeleń M., *Control Strategy of 1 kV Hybrid Active Power Filter for Mining Applications*, Energies, vol. 14, no. 16 (2021), DOI: 10.3390/en14164994.

[18] Li D., Wang T., Pan W., Ding X., Gong J., *A comprehensive review of improving power quality using active power filters*, Electric Power Systems Research, vol. 199, 107389 (2021), DOI: 10.1016/j.epsr.2021.107389.

[19] Zhang S., Ling B., Yang T., Hu H., Gao L., Zhou P., *Stability Analysis and Design of the Current Controller based on Generalized Delayed Signal Cancellation for LCL Active Power Filters*, in 2021 IEEE 1st International Power Electronics and Application Symposium (PEAS), pp. 1–5 (2021), DOI: 10.1109/PEAS53589.2021.9628808.

[20] Zhang S., Chen C., Ling B., Li X., Lu D., Hu H., *A Generalized Harmonic Extraction Algorithm Based on Multi-Window Average Filter Under Synchronous Rotating Frame*, IEEE Transactions on Power Electronics, vol. 38, no. 3, pp. 3752–3764 (2023), DOI: 10.1109/TPEL.2022.3217942.

[21] Cieplinski Ł., Gulczynski A., *Active parallel compensation using a power supply with a tunable inductive filter*, Archives of Electrical Engineering, vol. 73, no. 2, pp. 337–353 (2024), DOI: 10.24425/aee.2024.149920.

[22] Mućko J., Grugel P., *Selected static characteristics of a parallel active power filter with feedback from the supply voltage*, Archives of Electrical Engineering, vol. 73, no. 1, pp. 37–50 (2024), DOI: 10.24425/aee.2024.148855.

[23] Jain R.K., Barry V.R., Gadiraju H.K.V., *An Effective Control Strategy for Single-Phase Single-Stage PV Grid-Tied Inverter Under Abnormal Grid Conditions*, IEEE Journal of Emerging and Selected Topics in Power Electronics, vol. 12, no. 2, pp. 1249–1260 (2024), DOI: 10.1109/JESTPE.2023.3321374.

[24] Nguyen H.T., Moursi M.S.E., Hosani K.A., Al-Sumaiti A.S., Durra A.A., *Independent Time-Delay Signal Cancellation for Fast Harmonic-Sequence Filters Targeting Arbitrary Sequences and Frequencies*, IEEE Transactions on Industrial Informatics, vol. 20, no. 7, pp. 9330–9342 (2024), DOI: 10.1109/TII.2024.3383510.

[25] Li C. *et al*., *Space Vector Modulation for SiC and Si Hybrid ANPC Converter in Medium-Voltage High-Speed Drive System*, IEEE Transactions on Power Electronics, vol. 35, no. 4, pp. 3390–3401 (2020), DOI: 10.1109/TPEL.2019.2934129.